Study of protein folding under native conditions by rapidly switching the hydrostatic pressure inside an NMR sample cell

Cyril Charlier[a], T. Reid Alderson[a], Joseph M. Courtney[a], Jinfa Ying[a], Philip Anfinrud[a,1], and Adriaan Bax[a,1]

[a]Laboratory of Chemical Physics, National Institute of Diabetes and Digestive and Kidney Diseases, National Institutes of Health, Bethesda, MD 20892-0520

Contributed by Adriaan Bax, March 21, 2018 (sent for review March 1, 2018; reviewed by Lewis E. Kay and Peter E. Wright)

In general, small proteins rapidly fold on the timescale of milliseconds or less. For proteins with a substantial volume difference between the folded and unfolded states, their thermodynamic equilibrium can be altered by varying the hydrostatic pressure. Using a pressure-sensitized mutant of ubiquitin, we demonstrate that rapidly switching the pressure within an NMR sample cell enables study of the unfolded protein under native conditions and, vice versa, study of the native protein under denaturing conditions. This approach makes it possible to record 2D and 3D NMR spectra of the unfolded protein at atmospheric pressure, providing residue-specific information on the folding process. ^{15}N and ^{13}C chemical shifts measured immediately after dropping the pressure from 2.5 kbar (favoring unfolding) to 1 bar (native) are close to the random-coil chemical shifts observed for a large, disordered peptide fragment of the protein. However, ^{15}N relaxation data show evidence for rapid exchange, on a ∼100-μs timescale, between the unfolded state and unstable, structured states that can be considered as failed folding events. The NMR data also provide direct evidence for parallel folding pathways, with approximately one-half of the protein molecules efficiently folding through an on-pathway kinetic intermediate, whereas the other half fold in a single step. At protein concentrations above ∼300 μM, oligomeric off-pathway intermediates compete with folding of the native state.

ubiquitin | protein folding | high pressure | NMR spectroscopy | folding intermediate

Many decades of experimental, computational, and theoretical studies have aimed to unravel the process by which an unfolded protein chain can switch to its native, uniquely folded state on a timescale that is many orders of magnitude faster than expected for a random process (1–8). Although much has been learned, fundamental differences in the proposed mechanisms continue to fuel debate about how, and to what extent, proteins fold via predetermined sequential steps (7), or via multiple alternate pathways on a low-dimensional free-energy surface (9–11). For many small proteins, a single barrier on the folding pathway, separating the unfolded from the folded state, suffices to explain a large variety of experimental data, mostly based on rapid mixing, stopped-flow experiments. For other, mostly larger systems, experimental evidence points to the presence of metastable intermediate species (4, 6, 11–16).

Although transient unfolding events can be monitored under static conditions by measurement of backbone amide hydrogen exchange (3, 17) or NMR relaxation dispersion under native or near-native conditions (18, 19), in most protein folding experiments sample conditions are typically changed abruptly from those favoring the unfolded state to those favoring the native state. This may be accomplished, for example, by a sudden jump in pH, dilution of denaturant concentration, or by an abrupt drop in hydrostatic pressure. The latter mode of switching is arguably the most benign, allowing the protein to be probed under native buffer conditions. However, population of the unfolded state at high pressure requires that the volume of the unfolded state is substantially smaller than that of the native state. Pressure jump fluorescence measurements have yielded many insights into the kinetics by which proteins switch between multiple intermediates during the folding process (20, 21). Positive and negative temperature jump experiments are also possible to change the relative population of folded and unfolded states, and novel rapid freezing experiments, followed by solid-state NMR analysis, were used to identify intermediate species for a protein generally considered to be a fast two-state folder (22).

NMR experiments, carried out at elevated hydrostatic pressure, permit simultaneous observation of the folded and unfolded states of a protein in equilibrium, and can yield residue-specific information on both states (23–25). Analogous to pressure jump fluorescence experiments, the temporal change in the NMR spectrum following a step change in pressure can reveal kinetic information, provided the kinetics are slower than the duration of the pressure change and the time needed to record an NMR spectrum (26). This latter limitation has been addressed by development of dedicated hardware that rapidly changes the pressure in the NMR sample cell in a process synchronized with the data acquisition process (27). The ability to repeat the pressure jump process many times then provides access to processes on timescales much shorter than those needed to collect an entire multidimensional NMR spectrum.

Nevertheless, it has proven to be difficult to safely jump the pressure in an NMR sample cell by kilobar amounts faster than the time required for protein folding. Recently, however, we succeeded in developing a system that is capable of rapidly (1–3 ms) switching back and forth between 1 bar and pressures as

Significance

Development of specialized instrumentation enables rapid switching of the hydrostatic pressure inside an operating NMR spectrometer. This technology allows observation of protein signals during the repeated folding process. Applied to ubiquitin, a previously extensively studied model of protein folding, the methodology reveals an initially highly dynamic state that deviates relatively little from random coil behavior but also provides evidence for numerous repeatedly failed folding events, previously only observed in computer simulations. Above room temperature, direct NMR evidence shows a ∼50% fraction of proteins folding through an on-pathway kinetic intermediate, thereby revealing two equally efficient parallel folding pathways.

Author contributions: C.C., T.R.A., J.Y., P.A., and A.B. designed research; C.C., T.R.A., P.A., and A.B. performed research; C.C., T.R.A., J.M.C., J.Y., P.A., and A.B. contributed new reagents/analytic tools; C.C., T.R.A., J.M.C., and A.B. analyzed data; and T.R.A., P.A., and A.B. wrote the paper.

Reviewers: L.E.K., University of Toronto; and P.E.W., The Scripps Research Institute.

The authors declare no conflict of interest.

[1]To whom correspondence may be addressed. Email: philip.anfinrud@nih.gov or bax@nih.gov.

This article contains supporting information online at www.pnas.org/lookup/suppl/doi:10.1073/pnas.1803642115/-/DCSupplemental.

Published online April 16, 2018.

high as 2.7 kbar. This process can be repeated tens of thousands of times, only limited by mechanical wear of the system.

With our hardware capabilities, we are now poised to address a number of seminal questions on protein folding. One of these concerns the nature of the unfolded state of a protein under high-pressure and native conditions. Does the pressure-denatured protein collapse into a compact structure once the pressure is dropped to atmospheric levels, analogous to what is observed by FRET and paramagnetic relaxation experiments when denaturant is removed (28, 29)? Are off-pathway oligomeric intermediates responsible for the often-observed multiexponential folding kinetics (30, 31)? Are the lifetimes and populations of pretransition-state conformations sufficiently high that they impact the relaxation behavior of the NMR signal? A related question—to what extent are backbone amides engaged in H-bonding before barrier crossing—was addressed in the first application of our pressure jump apparatus (32). For ubiquitin, we found that, except for the N-terminal β-hairpin motif, no significant protection against amide hydrogen exchange with solvent by H-bonding was detectable. Other properties also become directly measurable, without recourse to extrapolation or the use of destabilizing additives. For example, the directly measurable temperature dependence of the folding and unfolding rates provides activation energies, and the pressure dependence of the unfolding rate yields the activation volume of the transition state. More detailed structural questions likely will also become within reach. For example, it should become possible to measure interproton distances for transient intermediates, provided their populations during the folding process are sufficiently high. We also anticipate that it will be feasible to measure the changes in NMR chemical shifts during the folding process, thereby providing information on site-specific rates. More generally, our newly developed hardware provides access to a direct NMR study of kinetics in any chemical reaction or process whose equilibrium can be significantly perturbed by the change of a few kilobars of hydrostatic pressure.

Methods

Pressure Jump Apparatus. The apparatus controlling the hydrostatic pressure consists of a high-pressure reservoir of hydraulic fluid, either mineral oil or mineral spirit, that is connected through a spectrometer-controlled valve and stainless-steel tubing to the NMR sample cell (Fig. 1). In the open state of the high-pressure valve, the aqueous protein solution inside the NMR sample cell rapidly equilibrates its pressure with the oil reservoir, which itself is pressurized by a pneumatically driven pump. The NMR sample cell, made of zirconium oxide and purchased from Daedalus Innovations, has an inner diameter (i.d.) of 2.7 mm and an outer diameter of 5 mm, and is rated for pressures of up to 3 kbar (33). Operating pressures are typically somewhat lower (~2.5 kbar) to reduce wear on the overall system and fatigue of the sample cell. After the high-pressure valve has closed, the pressure in the NMR sample cell remains stable until a spectrometer-controlled low-pressure valve connects the transfer line to a vessel at atmospheric pressure. The aqueous protein solution is compressed by ~8% at 2.5 kbar, and the transducing fluid by ~12%; upon switching back to low pressure, the hydraulic fluid expands into the atmospheric-pressure vessel and is recycled back by the high-pressure pump into the high-pressure reservoir. Work associated with pressurizing the water in the NMR sample cell results in an adiabatic temperature jump of ~3 °C at 2.5 kbar; depressurization triggers a corresponding drop in temperature. The change in temperature of the more compressible and lower heat capacity transducing oil is considerably larger. Moreover, its high flow speed (up to 150 m/s) through the valve body and stainless-steel transfer tubing results in turbulent flow and significant frictional heating. Cooling of the pressurized fluid after the high-pressure valve has closed causes a modest drop of the pressure. Opening the high-pressure valve a second time compensates for this drop. To minimize oxidative processes, the hydraulic fluid is kept under a N_2 atmosphere. The valve opening speeds are high, resulting in rapid pressure changes at the pressure sensor immediately adjacent to these valves (~1 ms for the 10–90% transition of the sigmoidal pressure profile). The actual rate of pressure change in the NMR sample, as measured by the resonance frequency of water under unlocked conditions, can either be comparable when using large diameter (2-mm i.d.) tubing, or substantially slower when using a small diameter (e.g., 0.5-mm i.d.). The use of small-diameter tubing reduces the volume of compressed transducing fluid, thereby extending longevity of the pump, but

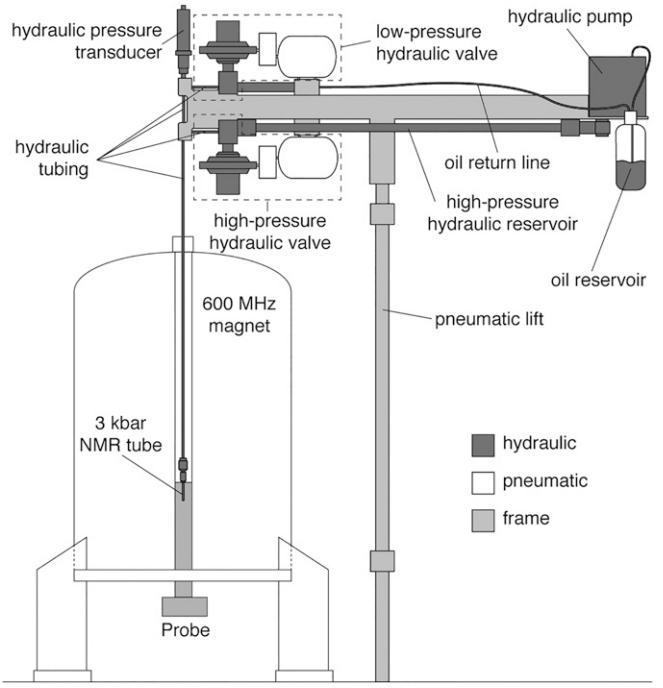

Fig. 1. Schematic representation of the pressure jump NMR apparatus. The protein solution is contained in a zirconia NMR sample tube, rated for 3 kbar of pressure, and is connected through stainless-steel tubing and a valve to a 125-mL reservoir containing pressurized hydraulic fluid (mineral oil or mineral spirits). A second valve connects the tubing to a vessel that is kept at 1 bar under an atmosphere of N_2 gas. Both air-activated valves are operated under spectrometer control. A hydraulic pump is used to recycle decompressed fluid back into the high-pressure reservoir. The entire assembly is mounted on a pneumatic lift for entry of the sample into the NMR magnet.

friction in the transfer line then limits the rate at which the NMR sample can be pressurized. When using large-diameter (2-mm) tubing for the transfer line, switching times for the low- to high-pressure transition approach 1 ms. However, with the ~8% compression of a 240-μL aqueous sample, the water–alkane interface will move by ~3.4 mm at a linear velocity of ~3.4 m/s. At 20 °C, this flow velocity corresponds to a Reynolds number of ~9,000, which is about 4.5 times the threshold where turbulence sets in. As a consequence, emulsification of the alkane-based hydraulic fluid into the protein sample can become visible after several hundred pressure cycles. For noncritical applications, where slower switching speeds suffice, we therefore opt to use narrower diameter (1-mm i.d.) tubing, which affords switching times in the 3- to 5-ms range.

Protein Expression and Purification. Experiments were carried out on a double mutant (V17A; V26A) of human ubiquitin. These mutations do not significantly affect the structure of the folded protein, as judged by nearly indistinguishable backbone chemical shifts relative to the wild-type protein (32) (*SI Appendix*, Table S1), but the increased volume difference between the folded and unfolded states makes the protein more amenable to pressure-induced unfolding (34): While wild-type ubiquitin requires more than 5 kbar to unfold (35), this midpoint of unfolding is shifted down to ~1.4 kbar (at 25 °C) for the cavity mutant. The protein was expressed and purified as described previously (32). While unfolded at high pressure, the protein is highly susceptible to cleavage by even trace contamination with cellular proteases. To eliminate this contamination, it was essential to employ an HPLC step in the purification protocol.

To compare the NMR characteristics of the protein in its unfolded state to that of a polypeptide incapable of forming a folded structure, we also expressed a fusion construct comprising hexahistidine-tagged GB1 followed by a short linker and then residues 19–76 of ubiquitin. A tobacco etch virus (TEV) protease cleavage site was included between the linker and the start of the ubiquitin sequence. The sample was purified by nickel affinity and the tag was removed upon incubation with TEV protease, which left a residual Gly residue at the N terminus. After cleavage, the fragment comprising

residues 19–76 was further purified by reverse nickel affinity, size exclusion, and HPLC.

NMR Spectroscopy. NMR spectra were recorded with standard heteronuclear 2D and 3D NMR experiments, slightly modified to keep the timing between the pressure jumps and the start of ^{1}H data acquisition constant when incrementing the indirect evolution periods. In practice, the minimum time needed between successive pressure cycles is about 8 s. This minimum is needed to avoid excessive heating, to bring the high-pressure reservoir back to its fully charged level, to reequilibrate any undulations at the interface between the hydraulic fluid (mineral oil) and the aqueous protein sample, and to establish a stable field-frequency lock on the NMR spectrometer. This longer than usual repetition time, combined with a maximum number of pressure cycles of ~15,000 between requisite maintenance of the high-pressure valve, limits the acquisition times in the indirect dimensions of 3D NMR experiments when recorded with standard sequential sampling protocols, leading to low spectral resolution. This problem can be mitigated by the use of nonuniform sampling protocols (36), typically using a sampling sparsity in the 5–25% range. For spectral reconstruction, we relied on the recently introduced SMILE software (37), integrated into the NMRPipe package (38).

Results

Apparent Two-State Kinetics of Ubiquitin Folding and Unfolding at Low Temperature. Folding of our ubiquitin double mutant is slow on the NMR timescale, which allows the simultaneous observation of separate signals for the unfolded and folded state, with each residue then represented by its unique resonance in the 2D NMR spectrum. Following a rapid drop in pressure from 2.5 kbar to 1 bar, the rate at which the NMR signals of the unfolded protein disappear, and the folded resonances reappear, is then readily tracked by recording a set of 2D heteronuclear single-quantum correlation (HSQC) experiments. Conversely, unfolding is monitored by recording spectra after the jump back to high pressure. Because folding is much faster than the time needed to acquire a complete 2D spectrum, only a single free induction decay (FID) is acquired at any given time point, τ, after each pressure switch. The final 2D spectrum, generated from many such FIDs, then identifies the state of each residue at time τ. At lower temperature, below ~15 °C, where rates of folding at low pressure and unfolding at high pressure are comparable to or slower than the time between consecutive scans in a regular 2D NMR experiment (~2 s), it is advantageous to record multiple HSQC spectra in an interleaved manner. In this case, if FIDs of the first HSQC spectrum are recorded at time τ_a after each pressure drop, $N-1$ additional FIDs can be recorded at times $\tau_a + n\mathrm{T}$, where $n = 1, \ldots, N-1$, and $\mathrm{T} \sim 2$ s (Fig. 2*A*). This then yields N 2D HSQC spectra that report on the intensity of a given resonance at time points $\tau_a + n\mathrm{T}$ after the pressure drop. As part of the same cycle, to monitor unfolding at high pressure, an additional M FIDs can be recorded at times $\tau_a + m\mathrm{T}$ after the pressure is jumped to high, where $m = 0, 1, 2, \ldots, M-1$ (Fig. 2*A*).

As can be seen (Fig. 2 *B* and *D*), high-quality HSQC spectra can be recorded by using the pressure jump apparatus in conjunction with a cryogenically cooled NMR probe head, which increases the sensitivity of the NMR signal. At 5 °C, the appearance of folded signals after a sudden drop to low pressure occurs at a rate that is slightly slower than the rate at which the unfolded resonances disappear, suggesting the possible presence of transient, NMR-invisible intermediates (Fig. 2*C*). For the unfolding transition, the rates are indistinguishable, indicating the absence of any intermediates (Fig. 2*E*).

Ubiquitin Folding and Unfolding Above Room Temperature. The rates at which the protein folds and unfolds after a pressure jump are strongly temperature dependent (see below), and above room temperature the folding rate becomes fast relative to the time required between collection of consecutive FIDs, making the recording of a time series of the type shown in Fig. 2*A* ineffective. In particular, the rapid disappearance of the unfolded spectrum after the pressure is dropped removes the advantage of recording multiple FIDs for each pressure cycle (*SI Appendix*, Fig. S1). To provide NMR access to the faster folding regime, we therefore rely on a variation of the zz-exchange experiment (39–41). Here, while the protein is pressure-denatured, ^{1}H spin magnetization is first efficiently transferred to longitudinal ^{15}N magnetization (Fig. 3*A*), thereby taking advantage of the favorable relaxation properties of the unfolded state. At time τ_d after the drop in pressure, the ^{15}N angular resonance frequency, ω_N, is encoded during a short evolution period, t_1, after which either a $\cos(\omega_N t_1)$ or $\sin(\omega_N t_1)$ of this magnetization is stored back along the z axis for a duration $\mathrm{T} - \tau_d - t_1$. At time T after the pressure drop, ^{15}N magnetization is then transferred back to the amide proton for observation, and time T is chosen sufficiently long (330 ms) such that most of the protein has returned to its folded, native structure at this time point. Importantly, the start of ^{1}H observation occurs always at the same total time after the initial pressure drop, ensuring that the observed $^1\mathrm{H}^N$ signals are solely modulated by the frequency of their attached ^{15}N nuclei at time τ_d, and not by any vibrational or temperature instabilities associated with the pressure jump. As can be seen, high-quality spectra can be recorded and show the exponential decay of unfolded protein (red), with a remarkably uniform time constant of 74 ± 3 ms (Fig. 3*G*). Recovery of the folded state (blue) appears approximately monoexponential but occurs at a considerably slower rate (~150 ms). The faster loss of unfolded signal than the recovery of folded signal points to the presence of one or more NMR-invisible intermediate states that are broadened by rapid transverse relaxation. Residue K11, located in a dynamically disordered loop region in the folded state, whose folded ^{15}N frequency falls very close to that of the unfolded state, appears to show a weak signal at an intermediate frequency at early points during the folding process (Fig. 3 *C* and *D*), supporting the presence of an intermediate state that is impacted by exchange broadening. This more complex, multistate folding behavior agrees with a range of prior hydrogen exchange and fluorescence studies (32, 42, 43), but is not seen in other analyses (44, 45). However, as our results indicate, and as discussed in more detail below, the maximum population of intermediate state(s) is strongly dependent on temperature and therefore can easily evade detection.

After a jump to high pressure, the rate at which the folded state disappears is comparable to the rate at which the unfolded state appears. This observation, made over a temperature range spanning 5–25 °C, suggests that high-pressure unfolding of ubiquitin is essentially a single barrier crossing event.

Temperature and Pressure Dependence of Folding and Unfolding Rates. The above pressure jump NMR experiment, when carried out at multiple temperatures, makes it straightforward to derive activation energies for the folding and unfolding process, at low and high pressure, respectively. Measurements taken at 5, 15, and 25 °C show a much steeper temperature dependence of the folding rates at low pressure (Fig. 4 *A* and *B*) than of the unfolding rates at high pressure (Fig. 4 *C* and *D*). To determine the folding/unfolding activation energies, E_A, the corresponding rates, $k(T)$, were fit to the Arrhenius equation:

$$k(T) = A\,\exp(-E_A/RT), \qquad [1]$$

where A is the fitted pre-exponential factor and R is the universal gas constant. The Arrhenius activation energy for the disappearance of unfolded state resonances at 1 bar (measured over a set of residues with well-resolved signals at all three temperatures) was found to be 21.9 ± 0.5 kcal/mol (see red line in Fig. 4*B*). The rate of appearance of the folded resonances does not fit well to standard Arrhenius behavior (Fig. 4*B*, dashed blue line), which is caused by deviations from two-state kinetics that become more visible above room temperature (see below). Our finding adds experimental data to the long-standing discussion regarding the origins of non-Arrhenius folding behavior (46, 47). We note that the fitted apparent activation energy for folding is similar to the value of 17.4 kcal/mol obtained from extrapolating the denaturant-dependent refolding rate, monitored by fluorescence on a F45W mutant (48).

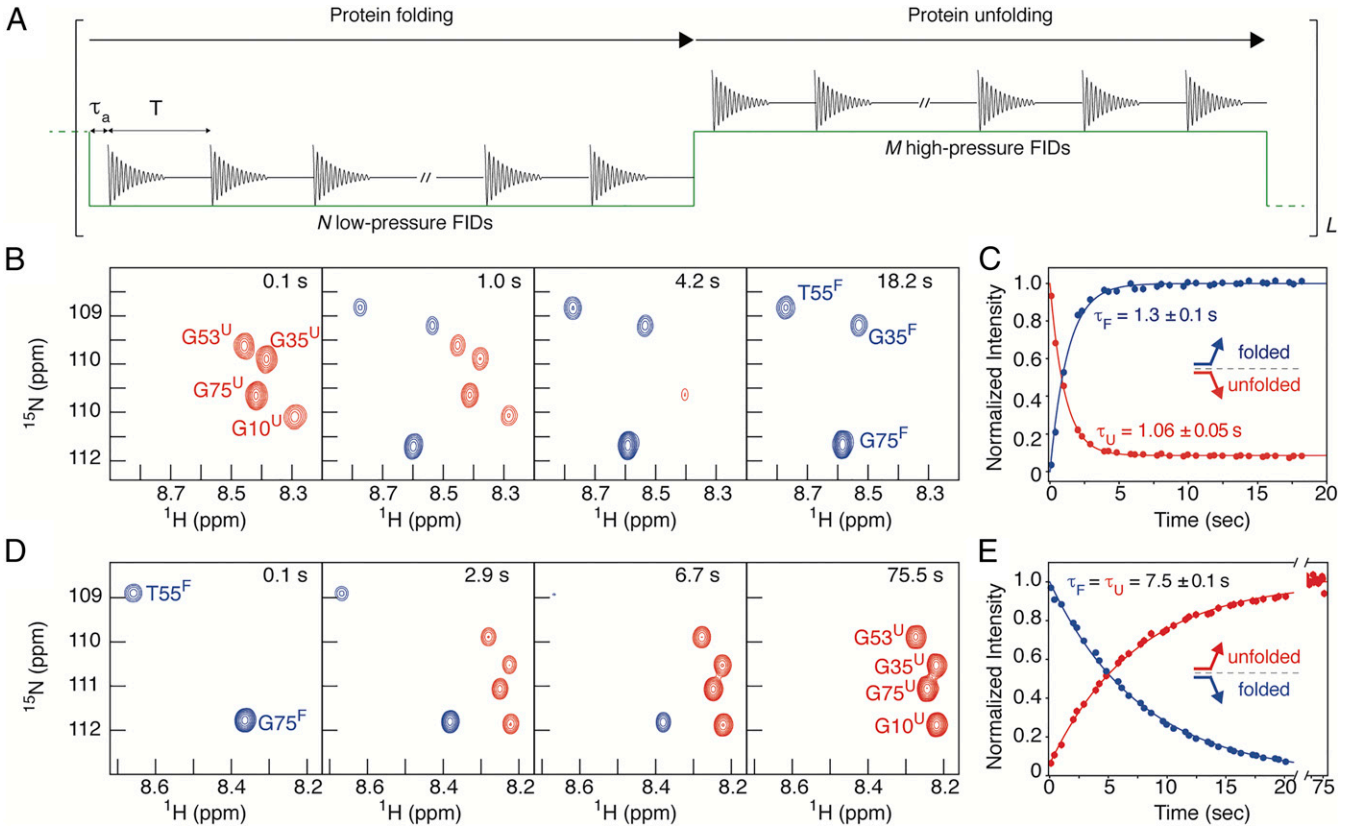

Fig. 2. Observation of protein folding and unfolding by NMR spectroscopy. (*A*) Schematic diagram of a time course experiment for the measurement of *N* successive low-pressure 2D HSQC spectra (and *M* high-pressure spectra) to follow the protein folding (unfolding) process on a residue-by-residue basis. Hydrostatic pressure is marked in green. At time points $\tau_a + n$T after each pressure switch, *N* (or *M*) FIDs are recorded, and collection of the entire series of FIDs is repeated *L* times, with *L* being the number of t_1 increments times the number of scans (typically 2) used for signal averaging. Final 2D NMR spectra then correspond to the state of the protein at times $\tau_a + n$T after the pressure switch. (*B*) Subset of the series of spectra recorded after the pressure was dropped to 1 bar to monitor the appearance of folded protein signals (blue) and the disappearance of the unfolded state resonances (red), with colors added manually. Residues are labeled by their one-letter residue code and number, with U and F denoting the unfolded and native state, respectively. (*C*) Time dependence of the resonance intensities of well-resolved cross-peaks. (*D* and *E*) Data analogous to *B* and *C* but monitoring the unfolding of the protein after pressure is jumped from 1 bar to 2.5 kbar. Spectra were recorded at 5 °C (set temperature at high pressure) for a sample containing 0.3 mM ubiquitin in 25 mM phosphate buffer, pH 6.4. The time dependence of signal appearance and disappearance at other temperatures and pressures is included in *SI Appendix*, Fig. S1.

Unfolding at 2.5 kbar yields the same value of 9.2 ± 0.2 kcal/mol when observing the disappearance of folded or appearance of unfolded resonances (Fig. 4 *C* and *D*). This value is in close agreement with single-molecule pulling experiments (8.4–11.0 kcal/mol) (48, 49).

As shown above, pressure-induced unfolding shows no evidence for intermediate(s) and therefore can be considered a two-state process with a single barrier separating folded and unfolded states. The pressure dependence of the unfolding rate then provides a direct measure for the difference in volume, ΔV_u^*, between the transition state and the folded state:

$$k(p) = A' \exp\left(-p\Delta V_u^*/RT\right). \quad [2]$$

For our ubiquitin mutant, the rate of unfolding increases with pressure (Fig. 4 *E* and *F*), corresponding to a ΔV_u^* difference of −26 ± 2 mL/mol, as measured from a global fit of the rates of appearance of the unfolded state and disappearance of the folded state (*SI Appendix*, Table S2).

Concentration Dependence of Ubiquitin Folding. The kinetic model for the folding of small proteins has been the subject of much debate. In particular, measurements of nonlinearity of the logarithm of the folding rate when plotted against denaturant concentration have been widely used as evidence for the presence of intermediates on the kinetic pathway (50–52). On the other hand, such nonlinearity also has been attributed to off-pathway oligomer formation or aggregation (30), even at low micromolar concentrations of F45W ubiquitin (31).

For quantitative measurements, our pressure jump NMR experiments use long recovery times between scans and small sample volumes and therefore require concentrations of greater than or equal to ∼100 μM. By contrast, single static measurements on pressure-denatured ubiquitin at 2.5 kbar are feasible down to concentrations of ∼1 μM. Such spectra, recorded at 800 MHz, show no detectable effect of concentration on the high-resolution HSQC spectrum (*SI Appendix*, Fig. S2). On the other hand, our previous study of the refolding kinetics probed by hydrogen exchange showed biexponential recovery of the native spectrum, with the more slowly recovering fraction of protein attributed to an oligomeric off-pathway intermediate (32).

Here, we have monitored the refolding kinetics for sample concentrations ranging from 150 to 900 μM. The strong concentration dependence of the fraction of protein that exhibits rapid refolding, monitored by either its amide intensity or the intensity of the L50 $C^{\delta 2}$ methyl group that resonates far upfield in the folded state, confirms the presence of one or more off-pathway oligomeric intermediates (Fig. 5 *A* and *B*). At concentrations above ∼1 mM, a fraction of protein does not refold when the pressure is suddenly dropped; for example, even when starting with soluble, well-folded ubiquitin at 3 mM, the concentration of protein that refolds after multiple cycles is just ∼1 mM. Below 1 mM, the recovery of folded signals is well fitted

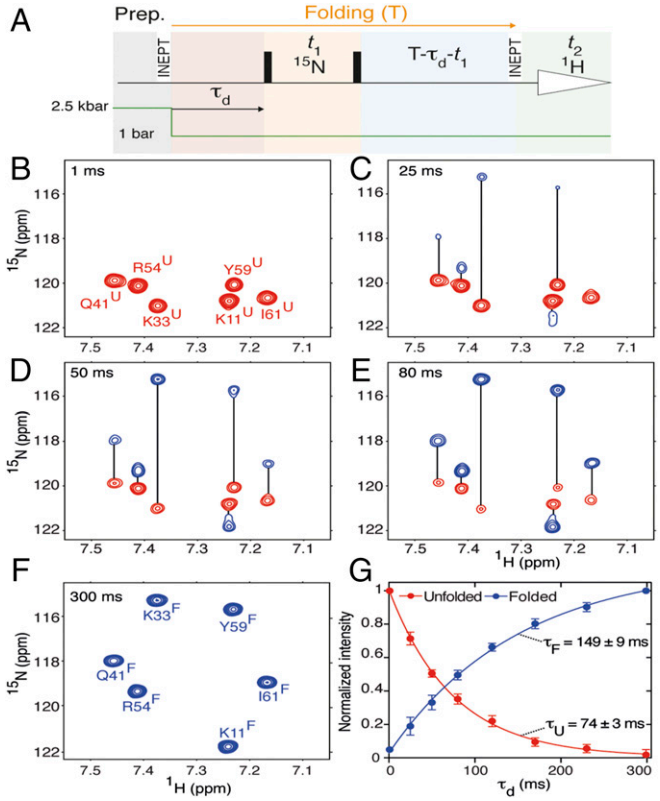

Fig. 3. Observation of protein folding by zz-exchange spectroscopy. (*A*) Schematic timing diagram of the pulse sequence. At the end of a high-pressure equilibration period (12 s), the ^{1}H magnetization is transferred to $^{15}N_z$ magnetization by a refocused INEPT pulse scheme. Conversion to transverse ^{15}N magnetization and subsequent t_1 evolution, followed by a pulse that stores a $\cos(\omega_N t_1)$ fraction of this magnetization back to *z*, is initiated at time τ_d after the pressure drop, thereby encoding the ^{15}N frequencies present at τ_d. At a fixed time, T, after the pressure drop, this encoded ^{15}N magnetization is transferred back to the amide proton for ^{1}H detection. T is chosen sufficiently long (330 ms) that most of the protein has folded at the time of detection. (*B–F*) Small regions of the HSQC spectra, recorded on a 280 μM ^{2}H/^{15}N/^{13}C-enriched ubiquitin sample at indicated τ_d delay durations after the pressure drop. All spectra correlate the frequency of the detected amide proton in the folded protein to the ^{15}N frequency of either the unfolded (red) or folded (blue) protein, with resonance intensities proportional to the fractions populating the unfolded and native states. Note that colors have been added manually. Residues are labeled by their one-letter residue code and number, with U and F denoting the unfolded and native state, respectively. (*G*) Time dependence of the resonance intensities observed in *B–F*. Fitted time constants show faster disappearance of resonances of the unfolded state than appearance of the folded final spectrum.

by a biexponential function, with time constants of 370 ms and 3.5 s (at 15 °C). At 150 μM, the amplitude of the slowly recovering component is no longer detectable, and even at 300 μM it only corresponds to ∼5%. Most measurements were therefore carried out at 300 μM as a compromise between optimal sensitivity and minimizing off-pathway oligomerization. The absence of NMR signal intensity associated with the oligomeric component, even when it is present at concentrations higher than the visible monomeric fraction, indicates that fast relaxation prevents the efficient transfer of magnetization required for observation of HSQC spectra. This behavior is consistent with either a very large species for this off-pathway fraction, or an oligomer with extensive dynamics on a microsecond-to-millisecond timescale.

Long-Lived On-Pathway Folding Intermediate. The kinetic model of ubiquitin folding has been controversial, with early work concluding it to be a three-state folder, whereas later studies refuted this finding (31, 43, 45, 48, 53, 54). As measured here, the faster disappearance of the unfolded state resonances after the protein is switched to 1 bar (∼17/s) than the apparent rate at which the spectrum of the final folded state recovers (∼7/s) points to the presence of an intermediate, NMR-invisible species (Fig. 3). Observation of the methyl group signal of L50, which is upfield shifted to −0.3 ppm in the folded state due to its packing against the aromatic ring of Y59, provides unambiguous supporting evidence for a metastable folding intermediate. Because its observation does not require the relatively long, fixed delays needed for magnetization transfer used in the observation of amide signals, its signal intensity is less sensitive to exchange broadening, and a methyl group signal at −0.2 ppm with a lifetime of ∼70 ms at 25 °C is clearly visible at short times after the unfolded protein is switched to 1 bar (Fig. 5*C*). This resonance then rapidly converts, unidirectionally, to the previously assigned (55) L50-C$^{\delta 2}$H$_3$ group at −0.3 ppm of the fully folded protein (Fig. 5*D*), demonstrating unequivocally that the intermediate is on-pathway. Note that the asymmetry about the diagonal in the NOESY spectrum of Fig. 5*D*, also seen for other methyl resonances, is an inherent property of the nonequilibrium state under which the spectrum is recorded. A strong direct cross-peak between the unfolded and folded resonance of L50-C$^{\delta 2}$H$_3$ is also seen. A fit of the intensities observed for the intermediate and folded resonance intensities of L50-C$^{\delta 2}$H$_3$ to the kinetic scheme depicted in Fig. 5*C* yields comparable rate constants, $k_{U\text{-}F}$ and $k_{U\text{-}I}$, for the direct and intermediate pathways, that agree fairly well with the delayed appearance of the folded amide signals relative to the disappearance of their unfolded counterparts (Fig. 3). As expected, when the reverse rates for each transition in the kinetic scheme were included as variables in the fit, they invariably converged to zero during optimization.

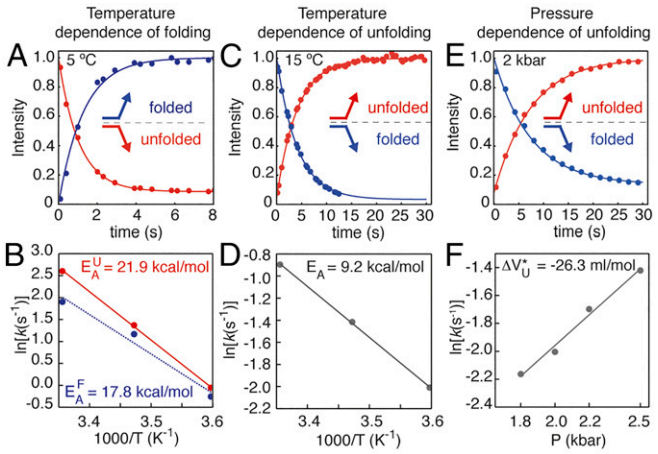

Fig. 4. Temperature and pressure dependence of ubiquitin folding and unfolding. (*A*) Disappearance of intensity of unfolded and appearance of folded protein signals as a function of time after the pressure is dropped from 2.5 kbar to 1 bar. Signal intensities are obtained with the scheme shown in Fig. 2 for a sample containing 0.3 mM ubiquitin, pH 6.4, at 5 °C. Intensities are averaged over a set of well-resolved resonances. Data for 15 and 25 °C are shown in *SI Appendix*, Fig. S1. (*B*) Arrhenius activation energies of ubiquitin folding, derived from the data shown in *A* and *SI Appendix*, Fig. S1. (*C*) Appearance of unfolded state and disappearance of folded state signals at 15 °C, 2.5 kbar. Data at 5 and 25 °C are shown in *SI Appendix*, Fig. S1. (*D*) Arrhenius activation energies of ubiquitin unfolding at 2.5 kbar, derived from the data shown in *C*. (*E* and *F*) Pressure dependence of ubiquitin unfolding at 15 °C. (*E*) Disappearance of folded protein signals and appearance of unfolded protein signals after jumping from atmospheric pressure to 2.0 kbar. Data measured at other pressures (1.8, 2.2, and 2.5 kbar) are shown in *SI Appendix*, Fig. S1C. (*F*) Plot of the protein unfolding rate against pressure, to derive the activation volume ΔV^*_U. Unfolding rates are obtained from the fits shown in *SI Appendix*, Fig. S1C. Scatter in the graph is dominated by uncertainty in the coarsely regulated pressure.

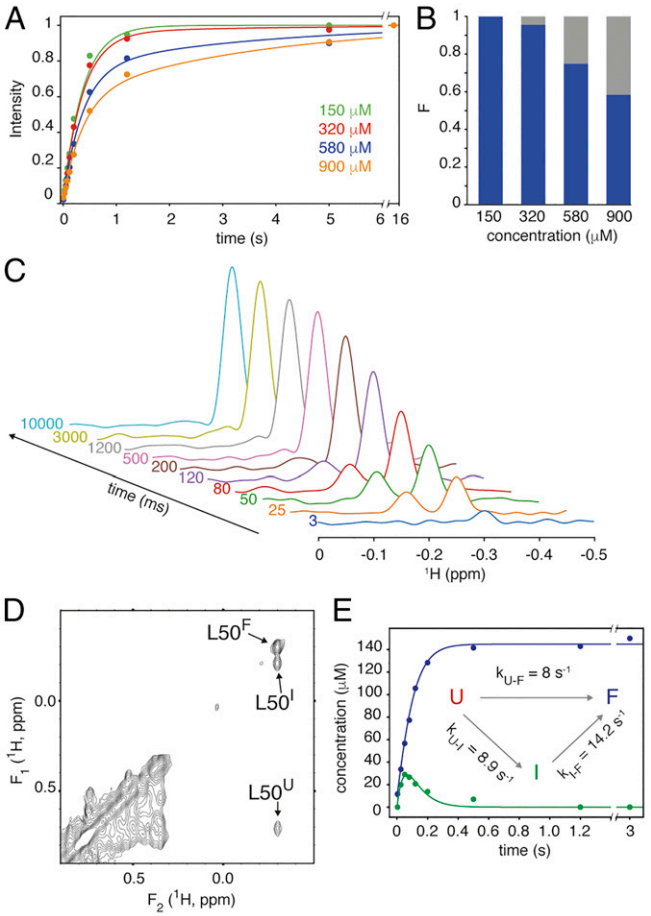

Fig. 5. Folding of ubiquitin as monitored by the $C^{\delta 2}H_3$ resonance of L50. (*A*) Concentration dependence of folding kinetics as monitored by the intensity, $I(t)$, of the native L50 $C^{\delta 2}H_3$ intensity at 15 °C. Solid lines are best fits to $I(t) = I(0) + F\,(1 - \exp(t/T_m)) + (1 - F - I(0))\,(1 - \exp(t/T_o))$, where F is the fraction folding with the fast time constant of the monomeric protein, $T_m = 370$ ms, and T_o is the time constant (3.54 s) of the slowly recovering fraction. $I(0)$ is the protein fraction that does not unfold at 2.5 kbar (~2.5%). (*B*) Partitioning of the monomeric (blue) and oligomeric (gray) fractions at various total protein concentrations. (*C*) Series of ^{1}H NMR spectra (150 μM, 25 °C), at indicated times after the pressure is dropped from 2.5 kbar to 1 bar. (*D*) Upfield region of a pressure jump 2D NOESY spectrum (100-ms mixing time), where the pressure drop occurs 40 ms before the start of ^{1}H t_1 evolution. The strong cross-peak between the F_1 frequency of the $L50^I$ $C^{\delta 2}H_3$ (at −0.2 ppm) and the native $L50^F$ $C^{\delta 2}H_3$ resonance (at −0.3 ppm) shows that the folding intermediate is on-pathway. (*E*) Intensity of the native L50 $C^{\delta 2}H_3$ resonance (blue) and the folding intermediate (green) as a function of refolding time. The intensity has been converted to concentration, using the intensity of the fully folded protein as a reference. Solid lines are the best-fit solutions calculated using the indicated rate constants.

At 5 °C, the on-pathway intermediate signal of L50-$C^{\delta 2}H_3$ remains visible but becomes less pronounced, reaching a maximum of only ~7% of the fully folded methyl intensity at 400 ms after the pressure is dropped to 1 bar. In the kinetic scheme of Fig. 5*C*, this indicates a much stronger temperature dependence of $k_{U\text{-}F}$ and $k_{U\text{-}I}$ than of $k_{I\text{-}F}$. This observation is consistent with the closer similarity of the rates at which unfolded state resonances disappear and folded state resonances appear below room temperature (Fig. 4*B*), and highlights the challenges in unambiguously identifying transient intermediate species, in particular when they are involved in parallel folding pathways.

Pressure-Denatured State. Having analyzed the kinetics of global folding and unfolding, we proceed to characterize the pressure-denatured state. Resonance assignments of the pressure-unfolded state (*SI Appendix*, Fig. S3*A* and Table S1) were made under static 2.5-kbar pressure by standard triple-resonance measurements as well as by the newly introduced pressure jump experiments (e.g., Figs. 3*A* and 6). After correction for the expected pressure dependence of chemical shifts in linear peptides (56, 57), shifts were found to be in fair, but not perfect agreement with predictions for random coil (*SI Appendix*, Fig. S3). Deviations from random coil chemical shifts, Δδ, often referred to as secondary chemical shifts, as well as deviations from random coil $^3J_{HNH\alpha}$ values (49), on average are slightly larger than those in urea-denatured wild-type ubiquitin (58). Positive Δδ values for $^{13}C^{\alpha}$ and $^{13}C'$ are sensitive indicators for an increased population of helical backbone torsion angles relative to a statistical coil distribution. Similarly, negative $\Delta^3J_{HNH\alpha}$ values ($\Delta^3J_{HNH\alpha} = {}^3J_{HNH\alpha}{}^{Unfolded} - {}^3J_{HNH\alpha}{}^{RandomCoil}$) point to an increased population of the helical and/or polyproline-2 (PPII) region of Ramachandran space, whereas positive values are indicative of a more extended backbone conformation. In contrast to urea-denatured ubiquitin at low pH, where secondary shifts show ~25% transient formation of the protein's N-terminal β-hairpin (59), pressure denaturation yields an unfolded state where $^{13}C^{\alpha}$ and $^{13}C'$ secondary chemical shifts for the N-terminal 18 residues are much closer to random coil and only show a very weak correlation with Δδ and $\Delta^3J_{HNH\alpha}$ values in the folded protein, indicating a population of less than 10% for the hairpin at 2.5 kbar (*SI Appendix*, Fig. S3*C*). However, positive $\Delta^3J_{HNH\alpha}$ values point to above average extended structure for this region in the pressure-denatured state at room temperature (*SI Appendix*, Fig. S3 *B* and *D* and Table S3). $^{13}C^{\alpha}$ and $^{13}C'$ chemical shifts are intrinsically less sensitive to increased β population than $^3J_{HNH\alpha}$ couplings, so these results are not inconsistent with one another. We note that $^3J_{HNH\alpha}$ couplings do not show a meaningful correlation with those in the native protein (*SI Appendix*, Fig. S3*D*). So, even though $^3J_{HNH\alpha}$ couplings suggest a slightly more extended structure than expected for random coil, this behavior does not appear to be dominated by transient β-hairpin formation at high pressure.

Small, positive $\Delta\delta^{13}C^{\alpha}$ and $\Delta\delta^{13}C'$ indicate elevated helical populations for three regions, I23–A28, Q41–F45, and Y59–V70, with close to random coil values for the remainder (*SI Appendix*, Fig. S3*A*). Negative $\Delta^3J_{HNH\alpha}$ values support increased helicity for these three segments (*SI Appendix*, Fig. S3*B*). The first region corresponds to the N-terminal half of ubiquitin's long α-helix in the native state (I23–G35). The other two regions adopt mostly β-strand structure in the native state, but previously were found to switch to the so-called A-state in the presence of methanol and/or high pressure and low temperature (60, 61). The current data show a similar trend, albeit with smaller amplitude, and with clear interruptions between the three helical segments.

The spectrum of the pressure-denatured state also shows nearly perfect superposition on that of the C-terminal fragment encompassing residues 19–76, both recorded at 2.5 kbar (*SI Appendix*, Fig. S4*A*). Only small upfield ^{15}N shift changes for residues 22–24 in the full-length protein relative to the peptide fragment point to transient interactions between these residues and those in the N-terminal segment.

Unfolded State at Atmospheric Pressure. The pressure jump apparatus enables measurement of ^1H, ^{13}C, and ^{15}N chemical shifts of the unfolded protein under native conditions, and it is of particular interest to investigate to what extent the not-yet-folded protein chain deviates from random-coil behavior. As mentioned above, NMR chemical shifts are particularly sensitive indicators for such deviations, whereas NMR relaxation measurements provide access to the chain dynamics in this unfolded state.

Carrying out 3D NMR experiments, where the first chemical shift evolution (^1H, ^{15}N, $^{13}C^{\alpha}$, or $^{13}C'$) of the unfolded protein is encoded immediately after the pressure drop, followed by a delay period (270 ms) to complete protein folding, allows the recording of spectra that correlate frequencies of these nuclei in

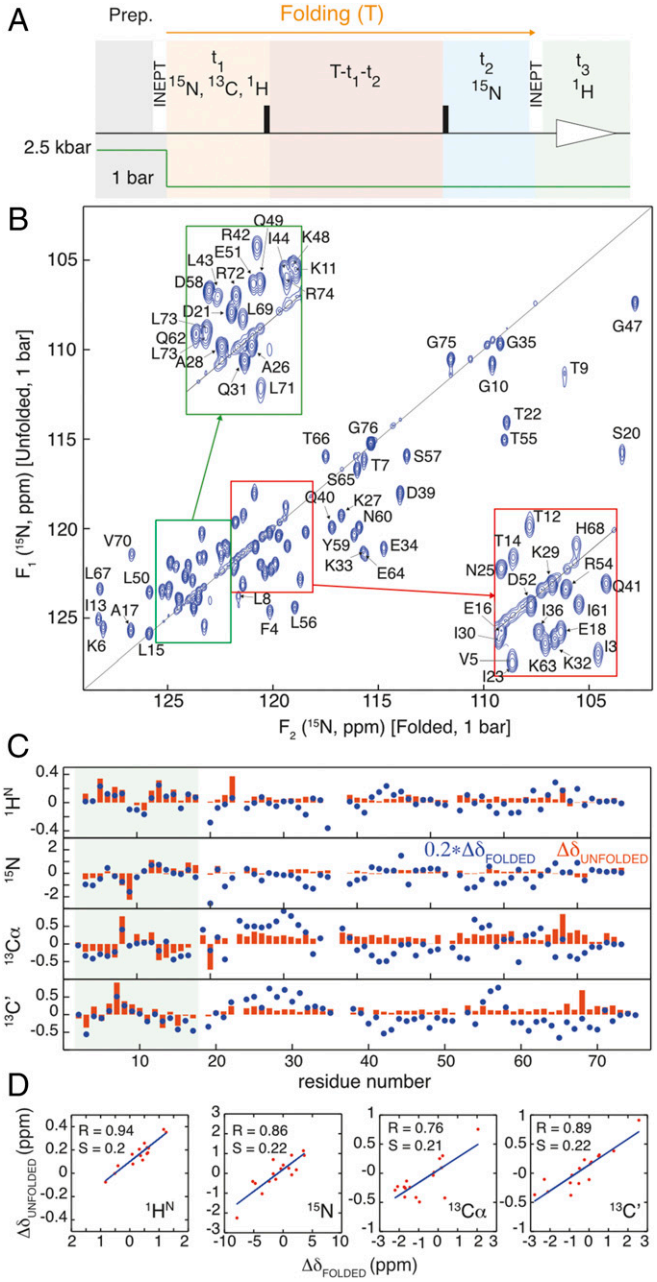

Fig. 6. Measurement of chemical shifts of unfolded ubiquitin at 1 bar, by 3D NMR. Data are recorded for a 300 μM sample of U(^{15}N,^{13}C,^{2}H) ubiquitin in 25 mM phosphate buffer, pH 6.4, 22 °C. (*A*) Schematic diagram of the pressure jump NMR experiment. The preparation period (Prep.) consists of a long delay (8 s) at high pressure, terminated by an efficient transfer of $^{1}H^{N}$ to *z* magnetization of either ^{15}N, or the ^{13}C′ or $^{13}C^{\alpha}$ of the preceding residue. For measurement of unfolded $^{1}H^{N}$ frequencies at 1 bar, the $^{1}H^{N}$ t_1 evolution period starts immediately after the pressure drop, and precedes transfer to ^{15}N. Immediately after the pressure drop, $^{1}H^{N}$, ^{15}N, ^{13}C′, or $^{13}C^{\alpha}$ evolution (t_1) modulates this *z* magnetization by $\cos(\omega_X t_1)$ or $\sin(\omega_X t_1)$, where $X = {}^{1}H^{N}$, ^{15}N, ^{13}C′, or $^{13}C^{\alpha}$, followed by transfer of X_z to in-phase $^{15}N_z$ magnetization. At time T = 270 ms after the pressure drop, ^{15}N magnetization (following a t_2 evolution period) is transferred to $^{1}H^{N}$ for detection. Note that ^{1}H detection starts always at the same time point, T, after the initial pressure drop. (*B*) Projection of the 3D [$^{15}N_{unfolded}$, $^{15}N_{folded}$, $^{1}H_{folded}$] spectrum on the $^{15}N_{unfolded}$–$^{15}N_{folded}$ plane, correlating the ^{15}N chemical shifts in the unfolded and folded states. (*C*) Experimental secondary chemical shifts in parts per million for the unfolded protein at 1 bar (orange bars, $\Delta\delta_{unfolded}$). For comparison; the secondary chemical shifts of the folded protein, scaled down by a factor of 5, are also shown (blue points, $\Delta\delta_{folded}$). The secondary chemical shifts are calculated relative to values of the pressure-denatured state at 2.5 kbar, adjusted to 1 bar using the random-coil pressure dependence values of Kalbitzer and coworkers (56, 57). (*D*) Correlation plots for residues 2–18 between the unfolded 1-bar secondary chemical shifts (*y* axis) and folded 1-bar secondary chemical shifts (*x* axis). The Pearson correlation coefficient, *R*, and the slope *S* of a linear regression analysis are marked in each panel.

the unfolded protein with those of the folded protein (Fig. 6). Although the unfolded ^{1}H, ^{15}N, $^{13}C^{\alpha}$, and ^{13}C′ chemical shifts measured in such a manner fall close to random-coil values, small but systematic differences are also seen (Fig. 6 *C* and *D*). For example, whereas $\Delta\delta^{13}C^{\alpha}$ and $\Delta\delta^{13}$C′ for the pressure-denatured protein correlated only weakly with the corresponding secondary chemical shifts in the native state (*SI Appendix*, Fig. S3), the 1-bar $\Delta\delta^{13}C^{\alpha}$ and $\Delta\delta^{13}$C′ values for the not-yet-folded protein, taken relative to the values in the pressure-denatured state, show a fair correlation with native structure secondary chemical shifts for the N-terminal 18 residues (Fig. 6*D*). A slope of 0.22 indicates a ∼22% increase in population of the N-terminal β-hairpin over that of the pressure-denatured protein.

Both experiments and molecular dynamics simulations point to formation of the N-terminal β-hairpin and its adjacent α-helix as the initial step in ubiquitin's folding process (62–65). Our unfolded state data at 1 bar support the propensity of residues 1–18 to form this antiparallel β-hairpin but do not show a significant increase in transient population of ubiquitin's native α-helix relative to the pressure-denatured state.

However, we do observe increased transient α-helix formation elsewhere in the protein. The small downfield $^{13}C^{\alpha}$ and ^{13}C′ secondary chemical shifts seen for segments Q39–F45 and L56–L71 at high pressure (*SI Appendix*, Fig. S3) become somewhat more pronounced at 1 bar, and now also include the region from A46–T55, forming essentially one very long contiguous α-helix as seen in the A-state (60, 61). Based on the magnitude of the secondary chemical shifts, the long C-terminal helix is populated at ∼20%. These results are consistent with the small but distinct increase in α-helicity seen by circular dichroism during the initial "burst phase" of ubiquitin folding (66), and may be considered a highly transient, off-pathway intermediate.

Evaluation of the chemical shifts in the manner described above yields information on the local structural propensity of the not-yet-folded protein at 1 bar. However, it does not unambiguously reveal the relation between these chemical shifts and interactions that may play a role in protein folding. For this reason, we also compare the 1-bar unfolded chemical shifts with those of a large C-terminal fragment of the protein, encompassing residues 19–76, which remains disordered at 1 bar (*SI Appendix*, Fig. S4) and therefore provides a reference for the local intrinsic structural propensity. Taking into account that the experimental uncertainties in the ^{1}H and ^{15}N shifts of the not-yet-folded full-length protein, extracted from the indirect dimension of a 3D spectrum, are considerably larger than those obtained from a static 2D HSQC spectrum, the agreement between the chemical shifts of the fragment and the full-length unfolded protein at 1 bar is remarkably close (*SI Appendix*, Fig. S4). Relative to the measurements made at 2.5 kbar, the only significant difference is seen for residues 25–34, which comprise the long α-helix in the folded protein. These residues show small but relatively uniform upfield ^{15}N chemical shift changes relative to the truncated construct and point to transient interactions with the N-terminal segment, which likely play a role in folding. By contrast, the above-noted α-helical propensity seen for the C-terminal half of the protein is an intrinsic property of the local sequence, present in both the fragment and full-length protein at 1 bar, and therefore not induced by interactions with the transiently present N-terminal hairpin.

Dynamics of the Unfolded Protein Under Native Conditions. Even though the unfolded protein at 1 bar is traversing the "energy landscape funnel" along its trajectory to the native state, its resonances

remain very close to those of the pressure-denatured form. NMR spectroscopy, and in particular spin relaxation measurements, are well suited to probe the formation of transient species during this process (18, 67), but such experiments mostly have been restricted to stationary conditions that either favored the folded or unfolded states of the protein. Pressure jump experiments permit the measurements to be carried out on the unfolded protein, under conditions where the equilibrium state is the fully folded protein.

Whereas the populations of local transient structure can be estimated from the chemical shifts, limits on their lifetimes can be established from ^{15}N transverse relaxation measurements. For this purpose, we carried out measurements where the protein is unfolded at high pressure, but briefly (for 125 ms) switched to low pressure while its ^{15}N transverse relaxation is recorded (Fig. 7*A*). Again, the time between the initial transfer of magnetization from ^{1}H to ^{15}N and the start of the ^{1}H detection period is kept constant. This means that when the ^{15}N magnetization is spin-locked for a variable duration, τ_{SL}, the ^{15}N storage time along the z axis is decreased by τ_{SL}. Therefore, the actual rate measured corresponds to the difference between the spin-locked transverse relaxation rate, $R_{1\rho}$, and the longitudinal relaxation rate, ^{15}N-R_1. The latter is slow and relatively uniform [~1.6 s^{-1} at 600-MHz ^{1}H frequency (68)] and therefore does not interfere with our analysis. To convert our experimental values to the true $R_{1\rho}$ relaxation rates, they were first increased by R_1, that is, by 1.6 s^{-1}. $R_{1\rho}$ values also were corrected for the effect of radio-frequency (RF) offset in the standard manner: $R_{1\rho} = (R_{1\rho}' - \sin^2\phi\, R_1)/\cos^2\phi$, where $R_{1\rho}'$ is the experimentally measured value, and $R_{1\rho}$ is the on-resonance value. Here, ϕ is the off-resonance angle: $\phi = \tan^{-1}(2\pi\delta/\omega_1)$, where δ is the ^{15}N resonance offset in hertz and ω_1 is the strength of the spin-lock RF field in angular frequency units. Note that $\sin^2\phi \leq 0.2$ for all our measurements, and errors resulting from the uniform $R_1 = 1.6$ s^{-1} assumption are negligible.

In the fast exchange limit where the residence time, τ', for a lowly populated ($p \ll 1$) transient on- or off-pathway intermediate is short relative to the frequency difference, $\Delta\omega$, between this transient structure and the unfolded chemical shift at 1 bar, the exchange contribution to the transverse relaxation is given by the following:

$$R_{1\rho,\mathrm{ex}} = p(1-p)(\Delta\omega)^2\tau' \Big/ \left[1 + (\omega_1\tau')^2\right]. \qquad [3]$$

Data collected at $\omega_1 = 2\pi \times 800$, $2\pi \times 1{,}250$, and $2\pi \times 2{,}000$ rad/s therefore are differentially impacted by the effect of conformational exchange, providing access to the timescale, τ', of the exchange process.

Measurements were carried out at 15 °C, where the rates of folding (~3 s^{-1}) and unfolding (~0.12 s^{-1}) are slow compared with the delay durations in the experiment. The actual ^{15}N signal evolution and ^{1}H detection take place after the sample is back at high pressure (Fig. 7*A*). The measured relaxation occurs at 1 bar, where the sample temperature is 3 °C lower due to the adiabatic decompression. The vast majority (>95%) of the ~30% fraction of proteins that fold during the 125-ms low-pressure period has insufficient time to unfold before ^{15}N evolution and ^{1}H detection, and therefore gives rise to separate resonances (corresponding to the folded protein at high pressure) in the detected spectrum. Our analysis focuses on the other fraction of proteins that did not fold during the low-pressure period and that exhibit unfolded chemical shifts during both ^{15}N evolution and ^{1}H detection. As can be seen (Fig. 7*B*), high-quality decay curves are obtained, which show considerable differences in rates among the various residues (*SI Appendix*, Table S4).

For most residues, ^{15}N relaxation times are remarkably long and approach the values measured in the static high-pressure denatured state (Fig. 7*C*). However, whereas at 2.5 kbar the relaxation rates are independent of spin-lock field strength (*SI Appendix*, Fig. S5 and Table S4), indicative of the absence of

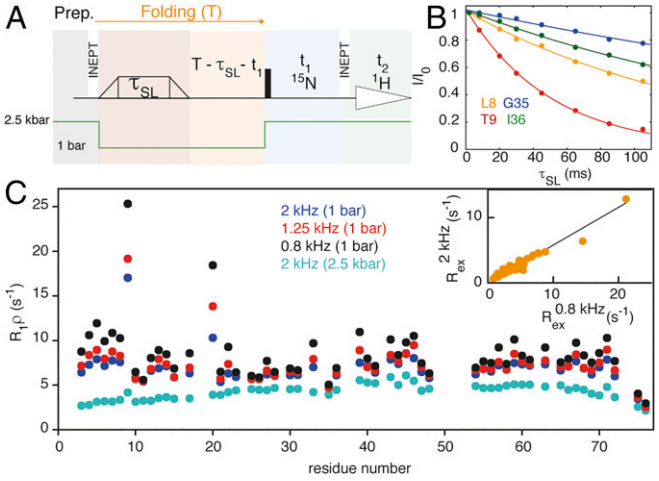

Fig. 7. Measurement of ^{15}N transverse relaxation in the unfolded state at 1 bar. (*A*) Schematic timing diagram of the pulse sequence. The preparation period (Prep.) consists of a high-pressure equilibration period (10 s) followed by transfer of ^{1}H magnetization to $^{15}N_z$ by a refocused INEPT pulse scheme. The pressure is then dropped to 1 bar for a fixed duration T (T = 125 ms). Immediately following the pressure drop, an adiabatic scheme is used to bring ^{15}N magnetization parallel to the spin-lock field for a variable duration τ_{SL}, before conversion back to the z axis. A pair of ^{1}H 180° pulses, applied at $\tau_{SL}/4$ and $3\tau_{SL}/4$, is used for removal of cross-correlated relaxation. When τ_{SL} is increased, the time for storage of ^{15}N along the z axis decreases, and the measured decay rate corresponds to $R_{1\rho} - R_1$. After the pressure is jumped back to 2.5 kbar, the amplitude of the $^{15}N_z$ magnetization is recorded as a regular 2D HSQC spectrum in the unfolded state. Note that this spectrum also contains resonances for the folded state, resulting from protein that folded during the low-pressure period, and has not yet unfolded at the time of ^{1}H detection. These signals are discarded. (*B*) Representative decay curves for selected residues, measured using a ^{15}N spin-lock field of 2 kHz for a 150 μM ^{15}N-labeled ubiquitin in standard buffer, with the sample temperature set to 15 °C, but the actual temperature being ~3 °C lower during the brief low-pressure period where the relaxation is actually measured. (*C*) ^{15}N relaxation rates for the unfolded protein at 1 bar. $R_{1\rho}$ rates shown have been derived from the fitted rates by removing the R_1 and offset contributions, as described in the text. Rates measured at three different spin-lock RF field strengths are all faster than seen at high pressure (aqua; *SI Appendix*, Fig. S4), indicative of conformational exchange contributions, R_{ex}, that scale with the strength of the spin-lock field (*Inset*). R_{ex} is calculated as $R_{ex} = R_{1\rho\,\mathrm{RF}}^{1\,\mathrm{bar}} - R_{1\rho\,2\,\mathrm{kHz}}^{2.5\,\mathrm{kbar}}$, where $R_{1\rho\,\mathrm{RF}}^{1\,\mathrm{bar}}$ is the rate measured in the pressure jump experiments at the indicated RF field strength, and $R_{1\rho\,2\,\mathrm{kHz}}^{2.5\,\mathrm{kbar}}$ is the $R_{1\rho}$ rate measured in the pressure-denatured state (2.5 kbar) using a 2-kHz spin-lock field.

conformational exchange processes on the >20-μs timescale, at 1 bar the transverse relaxation of the unfolded protein increases with decreasing spin-lock field strength. The difference in the transverse relaxation rates of the unfolded protein at 1 bar and 2.5 kbar must result from conformational exchange processes present in the thermodynamically unstable, unfolded state at 1 bar (Eq. **3**). Indeed, the exchange broadening seen at a spin-lock field strength of 800 Hz closely correlates with the $R_{1\rho,\mathrm{ex}}$ value at 2 kHz, and the slope of the correlation (Fig. 7*C*, *Inset*) yields $\tau' = 100$ μs for the timescale of the exchange process. With a Pearson correlation coefficient $R_P^2 = 0.5$, $R_{1\rho,\mathrm{ex}}$ does not show a strong correlation with the difference in ^{15}N resonance frequency between the folded and unfolded state at 1 bar. On the other hand, the observation that the exchange broadening seen at different spin-lock fields closely correlates across the entire protein (Fig. 7*C*, *Inset*) implies that the sampled energetic minima impact the ^{15}N chemical shifts of all residues that show R_{ex} contributions, that is, nearly all residues in the protein, and therefore are of a nature that is considerably more complex than simply the formation of local secondary structure. With $\tau' = 100$ μs determined from the spin-lock field dependence, and assuming average $\Delta\omega$ values of a few parts per million, representative of

chemical shift differences between folded structures and random-coil values, Eq. **3** yields a population for the transient species of $p \sim 3$–5%.

We note that $R_{1\rho}$ experiments are most sensitive to detection of motions in the 20- to 500-μs window. It is likely that transient structures with lifetimes shorter than 20 μs are also sampled by the protein during its folding process but remain invisible in our relaxation measurements. Transient structures with lifetimes longer than ∼500 μs may also be present but must be of low population considering that the free precession ^{15}N line widths of the unfolded protein at 1 bar are relatively narrow (*SI Appendix*, Fig. S6).

Discussion

Evaluating the detailed structure and dynamics of an unfolded protein under conditions where the native state is much more stable at equilibrium, that is, where it is in the process of folding, has long been of major interest to biophysics. The combination of rapid pressure jump technology with high-resolution NMR spectroscopy now offers a powerful approach to study the complete folding process in atomistic detail, as exemplified here for the previously well-studied ubiquitin protein.

In the pressure-denatured state, secondary chemical shifts show no significant correlation to those in the folded state and are very close to random-coil chemical shift values. ^{15}N transverse relaxation rates are also consistent with a dynamically highly disordered state, tracking values previously reported for the wild-type protein denatured in 8 M urea (68). The absence of significant protection of amide hydrogen exchange in the unfolded state similarly argues against a substantial population of intramolecular hydrogen bonding (32).

At first sight, the unfolded ubiquitin structure under native conditions behaves rather similar to the pressure-denatured state and to a fully disordered "random coil." Chemical shifts, which are excellent reporters on the local structure, show no drastic or abrupt changes when the pressure is decreased from denaturing (2.5-kbar) toward native (1-bar) conditions. Indeed, extrapolated 1-bar chemical shifts, using as input data measured for the pressure-dependent fraction of unfolded protein in a series of spectra recorded in the 1.0- to 2.5-kbar range, correlate fairly well with those measured on the unfolded protein at 1 bar by pressure jump NMR (*SI Appendix*, Fig. S7). However, we note that the nonlinearity of the pressure dependence of both the amide ^{1}H and ^{15}N chemical shifts is far larger than typically seen for unstructured linear peptides (*SI Appendix*, Fig. S7) (56). In particular, the nonlinearity of the pressure dependence of the chemical shifts in the unfolded state points to a shift in the conformational equilibrium as a function of pressure, and is considered a more sensitive indicator than the chemical shifts themselves (23). In fact, chemical shifts of the unfolded state at 1 bar point to a fractional population of the A-state, previously observed by unfolding in methanol or upon cold denaturation (60, 61). In the A-state, the C-terminal half of the protein forms a long α-helix, whereas it makes up three of ubiquitin's five-stranded β-sheet in the native state. Meanwhile, the N-terminal hairpin of the protein shows NMR chemical shifts and $^{3}J_{\mathrm{HNH}\alpha}$ couplings that correlate fairly well with the much larger deviations from random coil seen in the folded protein, indicative of a ∼20% transient population of this hairpin in the unfolded state at 1 bar, also seen in the A-state. The absence of a separate signature in our ^{15}N relaxation measurements for exchange between this substantially populated state and the disordered state indicates that the timescale for conversion back and forth into this hairpin conformation must be considerably faster than 20 μs. Indeed, formation of the structurally homologous β-hairpin of the Igg-binding domain of protein G was measured to be as fast as 6 μs by fluorescence (69).

Our transverse ^{15}N relaxation data indicate that the transient population of off-pathway intermediate species have lifetimes on the order of 100 μs. At 3–5%, the population of these transient structures is quite low and corresponds to their sampling about 400 times per second. Considering that the rate of crossing the free-energy barrier at 15 °C is ∼4/s, this implies that the protein undergoes ∼100 transitions to unproductive metastable energetic minima, before successfully crossing the first free-energy barrier. This behavior is predicted by all-atom molecular dynamics simulations that show "aborted folding attempts," where the chain appears to start its climb up the free-energy barrier, but either becomes transiently trapped in minima that do not provide a direct pathway to the transition state or lacks sufficient thermal energy to reach the transition state (65, 70, 71).

Our measurements additionally confirm the presence of oligomeric off-pathway intermediates when the refolding process takes place at concentrations above ∼300 μM. Above ∼1 mM, after multiple pressurization/depressurization cycles a fraction of this aggregated protein does not return to the folded monomeric state, even after long equilibration times.

Interestingly, our data shed light on the prior debate regarding the two- or three-state nature of ubiquitin's folding process. The observation of a separate transient signal for the upfield shifted C^{62} methyl signal shortly after the pressure is dropped to 1 bar provides strong evidence for an on-pathway folding intermediate. However, this pathway is in competition with a single-barrier pathway that occurs at a comparable rate. At lower temperature (5 °C), the maximum population of the intermediate never exceeds ∼7%, in agreement with its presence being detectable only at or above room temperature in the early fluorescence measurements by Roder and coworkers (48). More recent work by Vallée-Bélisle and Michnick (43, 53), using tryptophan-scanning mutagenesis, also provides compelling evidence for the late–folding-intermediate state. Our previous pressure jump study confirms that the late-state folding intermediate shows protection against amide hydrogen exchange with solvent that is very similar to that seen for the native protein, with the exception of several residues in the linker between ubiquitin's short 3_{10} helix and strand β5, which only become protected in the final native state (32).

Importantly, the on-pathway intermediate provides one of relatively few unambiguous experimental examples confirming theoretical work that proteins fold by parallel pathways (11). For ubiquitin, about one-half of the protein molecules reach their final folded state through this intermediate state, whereas the other half clears a single free-energy barrier. Our data therefore indicate that, contrary to the common view that regards intermediates as kinetic traps (16), three-state folding can be as efficient as two state. A detailed structural study of the intermediate, currently in progress, is challenging as even at room temperature its maximum population only reaches ∼20% of the total protein present in the sample (Fig. 5*E*), and its lifetime is short relative to typical times needed for buildup of the nuclear Overhauser effect.

ACKNOWLEDGMENTS. We thank J. L. Baber, Bernhard Howder, John M. Louis, and Gabriel Anfinrud for technical support, John Lloyd and the National Institute of Diabetes and Digestive and Kidney Diseases Core Facility for mass spectrometry, and William A. Eaton, G. Marius Clore, Dennis A. Torchia, and Robert Best for valuable discussions. This work was supported by the Intramural Research Program of the National Institute of Diabetes and Digestive and Kidney Diseases.

1. Dill KA, Chan HS (1997) From Levinthal to pathways to funnels. *Nat Struct Biol* 4: 10–19.
2. Kim PS, Baldwin RL (1990) Intermediates in the folding reactions of small proteins. *Annu Rev Biochem* 59:631–660.
3. Bai Y, Sosnick TR, Mayne L, Englander SW (1995) Protein folding intermediates: Native-state hydrogen exchange. *Science* 269:192–197.
4. Jennings PA, Wright PE (1993) Formation of a molten globule intermediate early in the kinetic folding pathway of apomyoglobin. *Science* 262:892–896.
5. Schuler B, Lipman EA, Eaton WA (2002) Probing the free-energy surface for protein folding with single-molecule fluorescence spectroscopy. *Nature* 419:743–747.
6. Walters BT, Mayne L, Hinshaw JR, Sosnick TR, Englander SW (2013) Folding of a large protein at high structural resolution. *Proc Natl Acad Sci USA* 110:18898–18903.
7. Englander SW, Mayne L (2017) The case for defined protein folding pathways. *Proc Natl Acad Sci USA* 114:8253–8258.
8. Plaxco KW, Simons KT, Baker D (1998) Contact order, transition state placement and the refolding rates of single domain proteins. *J Mol Biol* 277:985–994.

9. Piana S, Lindorff-Larsen K, Shaw DE (2011) How robust are protein folding simulations with respect to force field parameterization? *Biophys J* 100:L47–L49.
10. Henry ER, Best RB, Eaton WA (2013) Comparing a simple theoretical model for protein folding with all-atom molecular dynamics simulations. *Proc Natl Acad Sci USA* 110: 17880–17885.
11. Eaton WA, Wolynes PG (2017) Theory, simulations, and experiments show that proteins fold by multiple pathways. *Proc Natl Acad Sci USA* 114:E9759–E9760.
12. Roder H, Colón W (1997) Kinetic role of early intermediates in protein folding. *Curr Opin Struct Biol* 7:15–28.
13. Cecconi C, Shank EA, Bustamante C, Marqusee S (2005) Direct observation of the three-state folding of a single protein molecule. *Science* 309:2057–2060.
14. Neudecker P, et al. (2012) Structure of an intermediate state in protein folding and aggregation. *Science* 336:362–366.
15. Dyson HJ, Wright PE (2017) How does your protein fold? Elucidating the apomyoglobin folding pathway. *Acc Chem Res* 50:105–111.
16. Kiefhaber T (1995) Kinetic traps in lysozyme folding. *Proc Natl Acad Sci USA* 92: 9029–9033.
17. Englander SW, Mayne L (1992) Protein folding studied using hydrogen-exchange labeling and two-dimensional NMR. *Annu Rev Biophys Biomol Struct* 21:243–265.
18. Korzhnev DM, et al. (2004) Low-populated folding intermediates of Fyn SH3 characterized by relaxation dispersion NMR. *Nature* 430:586–590.
19. Korzhnev DM, Religa TL, Banachewicz W, Fersht AR, Kay LE (2010) A transient and low-populated protein-folding intermediate at atomic resolution. *Science* 329: 1312–1316.
20. Vidugiris GJA, Markley JL, Royer CA (1995) Evidence for a molten globule-like transition state in protein folding from determination of activation volumes. *Biochemistry* 34:4909–4912.
21. Wirth AJ, Liu Y, Prigozhin MB, Schulten K, Gruebele M (2015) Comparing fast pressure jump and temperature jump protein folding experiments and simulations. *J Am Chem Soc* 137:7152–7159.
22. Hu KN, Yau WM, Tycko R (2010) Detection of a transient intermediate in a rapid protein folding process by solid-state nuclear magnetic resonance. *J Am Chem Soc* 132:24–25.
23. Kitahara R, Hata K, Li H, Williamson MP, Akasaka K (2013) Pressure-induced chemical shifts as probes for conformational fluctuations in proteins. *Prog Nucl Magn Reson Spectrosc* 71:35–58.
24. Royer CA, et al. (1993) Effects of amino acid substitutions on the pressure denaturation of staphylococcal nuclease as monitored by fluorescence and nuclear magnetic resonance spectroscopy. *Biochemistry* 32:5222–5232.
25. Fu Y, et al. (2012) Coupled motion in proteins revealed by pressure perturbation. *J Am Chem Soc* 134:8543–8550.
26. Roche J, et al. (2013) Effect of internal cavities on folding rates and routes revealed by real-time pressure-jump NMR spectroscopy. *J Am Chem Soc* 135:14610–14618.
27. Kremer W, et al. (2011) Pulsed pressure perturbations, an extra dimension in NMR spectroscopy of proteins. *J Am Chem Soc* 133:13646–13651.
28. Aznauryan M, et al. (2016) Comprehensive structural and dynamical view of an unfolded protein from the combination of single-molecule FRET, NMR, and SAXS. *Proc Natl Acad Sci USA* 113:E5389–E5398.
29. Lipman EA, Schuler B, Bakajin O, Eaton WA (2003) Single-molecule measurement of protein folding kinetics. *Science* 301:1233–1235.
30. Silow M, Oliveberg M (1997) Transient aggregates in protein folding are easily mistaken for folding intermediates. *Proc Natl Acad Sci USA* 94:6084–6086.
31. Went HM, Benitez-Cardoza CG, Jackson SE (2004) Is an intermediate state populated on the folding pathway of ubiquitin? *FEBS Lett* 567:333–338.
32. Alderson TR, Charlier C, Torchia DA, Anfinrud P, Bax A (2017) Monitoring hydrogen exchange during protein folding by fast pressure jump NMR spectroscopy. *J Am Chem Soc* 139:11036–11039.
33. Peterson RW, Wand AJ (2005) Self-contained high-pressure cell, apparatus, and procedure for the preparation of encapsulated proteins dissolved in low viscosity fluids for nuclear magnetic resonance spectroscopy. *Rev Sci Instrum* 76:094101.
34. Roche J, et al. (2012) Remodeling of the folding free energy landscape of staphylococcal nuclease by cavity-creating mutations. *Biochemistry* 51:9535–9546.
35. Herberhold H, Winter R (2002) Temperature- and pressure-induced unfolding and refolding of ubiquitin: A static and kinetic Fourier transform infrared spectroscopy study. *Biochemistry* 41:2396–2401.
36. Mobli M, Hoch JC (2014) Nonuniform sampling and non-Fourier signal processing methods in multidimensional NMR. *Prog Nucl Magn Reson Spectrosc* 83:21–41.
37. Ying J, Delaglio F, Torchia DA, Bax A (2017) Sparse multidimensional iterative lineshape-enhanced (SMILE) reconstruction of both non-uniformly sampled and conventional NMR data. *J Biomol NMR* 68:101–118.
38. Delaglio F, et al. (1995) NMRPipe: A multidimensional spectral processing system based on UNIX pipes. *J Biomol NMR* 6:277–293.
39. Montelione GT, Wagner G (1989) 2D Chemical-exchange NMR-spectroscopy by proton-detected heteronuclear correlation. *J Am Chem Soc* 111:3096–3098.
40. Farrow NA, Zhang O, Forman-Kay JD, Kay LE (1994) A heteronuclear correlation experiment for simultaneous determination of ^{15}N longitudinal decay and chemical exchange rates of systems in slow equilibrium. *J Biomol NMR* 4:727–734.
41. Zhang Y, et al. (2016) High pressure ZZ-exchange NMR reveals key features of protein folding transition states. *J Am Chem Soc* 138:15260–15266.
42. Briggs MS, Roder H (1992) Early hydrogen-bonding events in the folding reaction of ubiquitin. *Proc Natl Acad Sci USA* 89:2017–2021.
43. Vallée-Bélisle A, Michnick SW (2012) Visualizing transient protein-folding intermediates by tryptophan-scanning mutagenesis. *Nat Struct Mol Biol* 19:731–736.
44. Went HM, Jackson SE (2005) Ubiquitin folds through a highly polarized transition state. *Protein Eng Des Sel* 18:229–237.
45. Krantz BA, Sosnick TR (2000) Distinguishing between two-state and three-state models for ubiquitin folding. *Biochemistry* 39:11696–11701.
46. Bryngelson JD, Onuchic JN, Socci ND, Wolynes PG (1995) Funnels, pathways, and the energy landscape of protein folding: A synthesis. *Proteins* 21:167–195.
47. Scalley ML, Baker D (1997) Protein folding kinetics exhibit an Arrhenius temperature dependence when corrected for the temperature dependence of protein stability. *Proc Natl Acad Sci USA* 94:10636–10640.
48. Khorasanizadeh S, Peters ID, Butt TR, Roder H (1993) Folding and stability of a tryptophan-containing mutant of ubiquitin. *Biochemistry* 32:7054–7063.
49. Garcia-Manyes S, Dougan L, Badilla CL, Brujic J, Fernández JM (2009) Direct observation of an ensemble of stable collapsed states in the mechanical folding of ubiquitin. *Proc Natl Acad Sci USA* 106:10534–10539.
50. Matouschek A, Kellis JT, Jr, Serrano L, Bycroft M, Fersht AR (1990) Transient folding intermediates characterized by protein engineering. *Nature* 346:440–445.
51. Muñoz V, Lopez EM, Jager M, Serrano L (1994) Kinetic characterization of the chemotactic protein from *Escherichia coli*, CheY. Kinetic analysis of the inverse hydrophobic effect. *Biochemistry* 33:5858–5866.
52. Khorasanizadeh S, Peters ID, Roder H (1996) Evidence for a three-state model of protein folding from kinetic analysis of ubiquitin variants with altered core residues. *Nat Struct Biol* 3:193–205.
53. Vallée-Bélisle A, Michnick SW (2007) Multiple tryptophan probes reveal that ubiquitin folds via a late misfolded intermediate. *J Mol Biol* 374:791–805.
54. Reddy G, Thirumalai D (2015) Dissecting ubiquitin folding using the self-organized polymer model. *J Phys Chem B* 119:11358–11370.
55. Di Stefano DL, Wand AJ (1987) Two-dimensional ^{1}H NMR study of human ubiquitin: A main chain directed assignment and structure analysis. *Biochemistry* 26:7272–7281.
56. Koehler J, et al. (2012) Pressure dependence of N-15 chemical shifts in model peptides Ac-Gly-Gly-X-Ala-NH_2. *Materials* 5:1774–1786.
57. Erlach MB, et al. (2016) Pressure dependence of backbone chemical shifts in the model peptides Ac-Gly-Gly-Xxx-Ala-NH_2. *J Biomol NMR* 65:65–77.
58. Meier S, Grzesiek S, Blackledge M (2007) Mapping the conformational landscape of urea-denatured ubiquitin using residual dipolar couplings. *J Am Chem Soc* 129: 9799–9807.
59. Meier S, Strohmeier M, Blackledge M, Grzesiek S (2007) Direct observation of dipolar couplings and hydrogen bonds across a beta-hairpin in 8 M urea. *J Am Chem Soc* 129: 754–755.
60. Brutscher B, Brüschweiler R, Ernst RR (1997) Backbone dynamics and structural characterization of the partially folded A state of ubiquitin by ^{1}H, ^{13}C, and ^{15}N nuclear magnetic resonance spectroscopy. *Biochemistry* 36:13043–13053.
61. Vajpai N, Nisius L, Wiktor M, Grzesiek S (2013) High-pressure NMR reveals close similarity between cold and alcohol protein denaturation in ubiquitin. *Proc Natl Acad Sci USA* 110:E368–E376.
62. Rea AM, Simpson ER, Meldrum JK, Williams HEL, Searle MS (2008) Aromatic residues engineered into the beta-turn nucleation site of ubiquitin lead to a complex folding landscape, non-native side-chain interactions, and kinetic traps. *Biochemistry* 47: 12910–12922.
63. Jourdan M, Searle MS (2000) Cooperative assembly of a nativelike ubiquitin structure through peptide fragment complexation: Energetics of peptide association and folding. *Biochemistry* 39:12355–12364.
64. Reddy G, Thirumalai D (2017) Collapse precedes folding in denaturant-dependent assembly of ubiquitin. *J Phys Chem B* 121:995–1009.
65. Piana S, Lindorff-Larsen K, Shaw DE (2013) Atomic-level description of ubiquitin folding. *Proc Natl Acad Sci USA* 110:5915–5920.
66. Larios E, Li JS, Schulten K, Kihara H, Gruebele M (2004) Multiple probes reveal a native-like intermediate during low-temperature refolding of ubiquitin. *J Mol Biol* 340:115–125.
67. Kukic P, et al. (2017) Structural characterization of the early events in the nucleation-condensation mechanism in a protein folding process. *J Am Chem Soc* 139:6899–6910.
68. Wirmer J, Peti W, Schwalbe H (2006) Motional properties of unfolded ubiquitin: A model for a random coil protein. *J Biomol NMR* 35:175–186.
69. Muñoz V, Thompson PA, Hofrichter J, Eaton WA (1997) Folding dynamics and mechanism of beta-hairpin formation. *Nature* 390:196–199.
70. Piana S, Klepeis JL, Shaw DE (2014) Assessing the accuracy of physical models used in protein-folding simulations: Quantitative evidence from long molecular dynamics simulations. *Curr Opin Struct Biol* 24:98–105.
71. Lindorff-Larsen K, Maragakis P, Piana S, Shaw DE (2016) Picosecond to millisecond structural dynamics in human ubiquitin. *J Phys Chem B* 120:8313–8320.